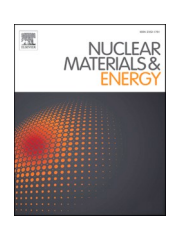
ELSEVIER

Contents lists available at ScienceDirect

# **Nuclear Materials and Energy**

journal homepage: www.elsevier.com/locate/nme





# X-ray and molecular dynamics study of the temperature-dependent structure of FLiNaK

Jicheng Guo <sup>a,1</sup>, Yifan Zhang <sup>b,1</sup>, Karl Ludwig <sup>c,d,\*,1</sup>, Haoxuan Yan <sup>d</sup>, Alexander Levy <sup>g</sup>, Anubhav Wadehra <sup>d</sup>, Michael C. Gao <sup>e</sup>, Chris Benmore <sup>f</sup>, Melissa Rose <sup>a</sup>, Nicholas Condon <sup>a</sup>, Adam Powell <sup>b</sup>, Yu Zhong <sup>b</sup>, Uday Pal <sup>d,g</sup>

- <sup>a</sup> Chemical and Fuel Cycle Technologies Division, Argonne National Laboratory, 9700 South Cass Avenue, Lemont, IL 60439, United States
- b Department of Mechanical and Materials Engineering, Worcester Polytechnic Institute, 100 Institute Rd., Worcester, MA 01609, United States
- <sup>c</sup> Department of Physics, Boston University, 590 Commonwealth Ave., Boston, MA 02215, United States
- d Division of Materials Science and Engineering, Boston University, 15 St. Mary's St., Boston, MA 02215, United States
- e U.S. Department of Energy National Energy Technology Laboratory, 1450 Queen Ave SW, Albany, OR 97321, USA
- f Advanced Photon Source, Argonne National Laboratory, 9700 South Cass Avenue, Lemont, IL 60439, United States
- g Department of Mechanical Engineering, Boston University, 15 St. Mary's St., Boston, MA 02215, United States

#### ARTICLE INFO

#### Keywords: Molten salt structure Molecular dynamics

# ABSTRACT

The atomic structure of FLiNaK and its evolution with temperature are examined with x-ray scattering and molecular dynamics (MD) simulations in the temperature range  $460-636\,^{\circ}$ C. In accord with previous studies, it's observed that the average nearest-neighbor (NN) cation-anion coordination number increases with increasing cation size, going from ~4 for Li-F to ~6.4 for K-F. In addition, we find that there is a coupled change in local coordination geometry – going from tetrahedral for Li-F to octahedral for Na to very disordered quasi-cuboidal for K. The varying geometry and coordination distances for the cation-anion pairs cause a relatively constant F-F next-nearest neighbor (NNN) distance of approximately 3.1 Å. This relatively fixed distance allows the F anions to assume an overall correlated structure very similar to that of a hard-sphere liquid with an extended radius which is beyond the normal F ion size but reflects the cation-anion coordination requirements. Careful consideration of the evolution of the experimental atomic distribution functions with increasing temperature shows that the changes in correlation at each distance can be understood within the context of broadening asymmetric neighbor distributions. Within the temperature range studied, the evolution of F-F correlations with increasing temperature is consistent with changes expected in a hard-sphere liquid simply due to decreasing density.

# 1. Introduction

Molten salts are of interest for a variety of energy applications, including as a coolant and fissile material carrier in molten salt reactors (MSRs) [1] and as an energy storage material in concentrated solar power stations [2]. The eutectic composition 46.5–11.5–42 mol % of LiF-NaF-KF, known as FLiNaK, has long been regarded as a model salt for MSR applications. Knowledge of the atomic structure of the liquid salt is important for understanding the origin of the material's physical and chemical properties. Accordingly, a number of x-ray [3,4] and neutron scattering [5] experiments, as well as molecular dynamics (MD) simulations [4,5,6], have examined the basic structure of molten FLiNaK, as

well as FLiNaK with added components [4,7,8]. These have focused primarily on nearest-neighbor coordination distances and numbers. Here, however, we take advantage of new x-ray scattering studies coordinated with MD simulations to investigate more deeply the structural motifs in the liquid beyond the coordination numbers. The present studies, examining temperatures from just above the melting point of 454 °C up to 636 °C, particularly focus on local coordination geometry and the importance and relative simplicity of the F-F correlations, which provide the largest single share of local atomic pairings due to the high atomic fraction of fluorine in the melt.

E-mail address: ludwig@bu.edu (K. Ludwig).

 $<sup>^{\</sup>star}$  Corresponding author.

<sup>&</sup>lt;sup>1</sup> Contributed equally.

#### 2. Experimental details

FLiNaK salt was prepared by melting the component salts (LiF, NaF and KF 46.5–11.5–42 mol %, Sigma Aldrich, >99% purity) in a ultrahigh purity argon glovebox and crushing the solidified salt into powders. The final composition was confirmed using Inductively-Coupled Plasma-Mass Spectroscopy (ICP-MS).

X-ray scattering experiments were performed at beamline 6-ID-D of the Advanced Photon Source using an x-ray energy of 100.3 keV. A Varex CT4343 area detector with 2880  $\times$  2880 150  $\mu m$  square pixels measured the scattered x-rays at a position 399 mm behind the sample. The scattering geometry was calibrated using a cerium dioxide powder sample. The sample furnace was as described in Guo  $\it et al.$  [9]. Samples were held in a glassy carbon crucible of 5 mm OD and 0.5 mm wall thickness which was held in a vacuum furnace chamber backfilled with +5 psi of Ar gas. Kapton windows were used for x-ray entrance and exit from the chamber.

Scattering from the FLiNaK was measured at 460 °C, 510 °C, 560 °C, 610 °C and 636 °C. Scattering from the empty glassy carbon crucible was also measured for subtraction from the total observed scattering. At each temperature five x-ray scans were performed, with each scan being 3000 frames of 0.1 s exposures, and then averaged.

# 3. Experimental results

The 2-d x-ray scattering data was circularly averaged over an appropriately masked area of the detector using Fit2D [10]. Background scattering was subtracted from the total scattering and the resulting FLiNaK scattering patterns were then analyzed using PDFGetX2 [11] with  $q_{min} = 0.60 \text{ Å}^{-1}$  and  $q_{max} = 16.0 \text{ Å}^{-1}$ . They were normalized to a per atom basis to obtain the structure factors S(q) and scattering functions F(q):

$$F(q) \equiv q[S(q) - 1] = q \left[ \frac{I(q)}{\langle f(q) \rangle^2} - \frac{\langle f^2(q) \rangle - \langle f(q) \rangle^2}{\langle f(q) \rangle^2} - 1 \right]$$
 (1)

Here the averages are over the atomic species  $\alpha$ , of concentrations  $c_{\alpha}$ , and the  $f_{\alpha}(q)$  are the atomic scattering factors for the given atomic species. The second term on the right-hand-side is the Laue diffuse scattering. Experimental results extrapolated to q=0 and multiplied by a Lorch function  $\sin(\Delta_0q)/(\Delta_0q)$  with  $\Delta_0=\pi/q_{max}$  [12] to minimize truncation oscillations in subsequent Fourier sine transforms are shown in Fig. 1. It can be noted that there are some unusual small features in the experimental F(q) curves in the range of 5–5.5 A<sup>-1</sup> and near 6.6 Å<sup>-1</sup>. These seem to be related to imperfect background subtraction and do not

affect the final quality of the results.

The scattering functions F(q) are related to the real-space distribution functions by:

$$F(q) = \sum_{\alpha,\beta} \frac{c_{\alpha}c_{\beta}f_{\alpha}(q)f_{\beta}^{*}(q)}{\langle f(q)\rangle^{2}} \rho_{0} \int 4\pi r \left[g_{\alpha\beta}(r) - 1\right] \sin qr dr \tag{2}$$

where  $\rho_0$  is the atomic density and the species-specific pair distribution functions  $g_{a\theta}(r)$  are:

$$g_{\alpha\beta}(r) \equiv \frac{1}{4\pi c_{\alpha} c_{\beta} N \rho_{0} r^{2}} \sum_{\substack{i \in \{\alpha\}\\ j \in \{\beta\}\\ i \neq j}} \delta(r - r_{ij})$$

$$(3)$$

where N is the total number of atoms. Because of the concentration- and scattering factor-dependence shown in Eq. (2), the strongest contributions to the x-ray scattering are from F-F, K-F and K-K correlations while Li-Li, Li-Na and Na-Na contributions are quite small.

In the Hannon-Howells-Soper (HHS) formalism [13], the differential correlation function is the sine transform of F(q):

$$D(r) = \frac{2}{\pi} \int_{0}^{\infty} F(q) \sin q r dq \tag{4}$$

The experimental differential correlation functions are shown in Fig. 2. For comparison, the tabulated results of Igarashi *et al.* [3] taken at 520 °C are also shown in Fig. 2. They are in good agreement with the present results at 510 °C. The D(r) function removes the average density and is particularly useful for examining structure on length scales beyond nearest neighbor. For future reference, we note that for visualization of structure at short distances, it's often useful to examine the total correlation function:

$$T(r) = 4\pi r \rho_0 + \frac{2}{\pi} \int_0^\infty F(q) \sin q r dq$$
 (5)

Atomic densities are calculated from the mass densities of Chernková  $et\ al.\ [14]$ . The experimental T(r) function for  $510\,^\circ\mathrm{C}$  at low separations r is shown in Fig. 3. The shortest correlations in the melt are from Li-F, Na-F and K-F nearest-neighbor (NN) distances. Due to the overlap between different atomic pair contributions, only the Li-F correlations appear distinctly, as a strong shoulder at a distance of approximately  $1.9\,\mathrm{\mathring{A}}$  on the background of Na-F and K-F correlations. In principle the individual contributions to T(r) can be fit, but the multiple contributions make this difficult to do in a reliable manner. We therefore refrain from trying to fit atomic shells directly to the measured distribution function and

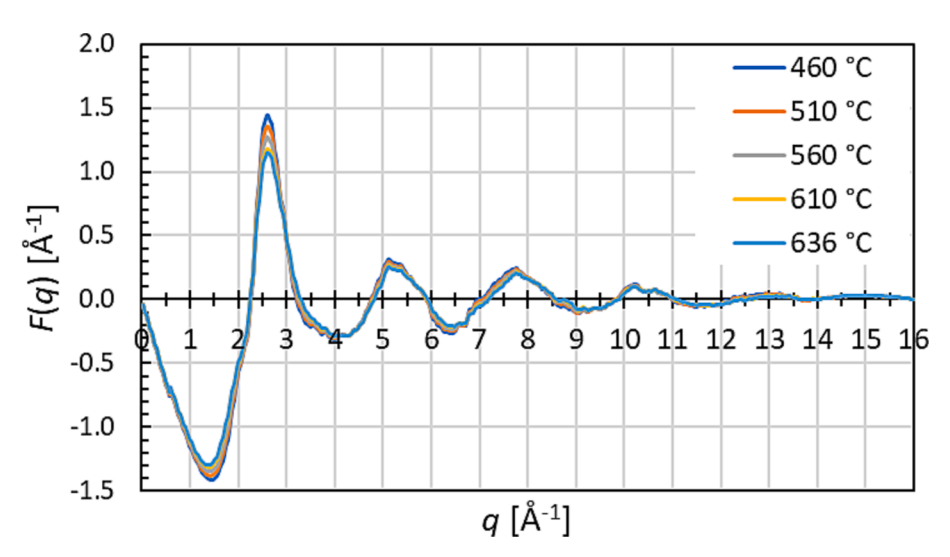


**Fig. 1.** Evolution of x-ray scattering function F(q) with temperature.

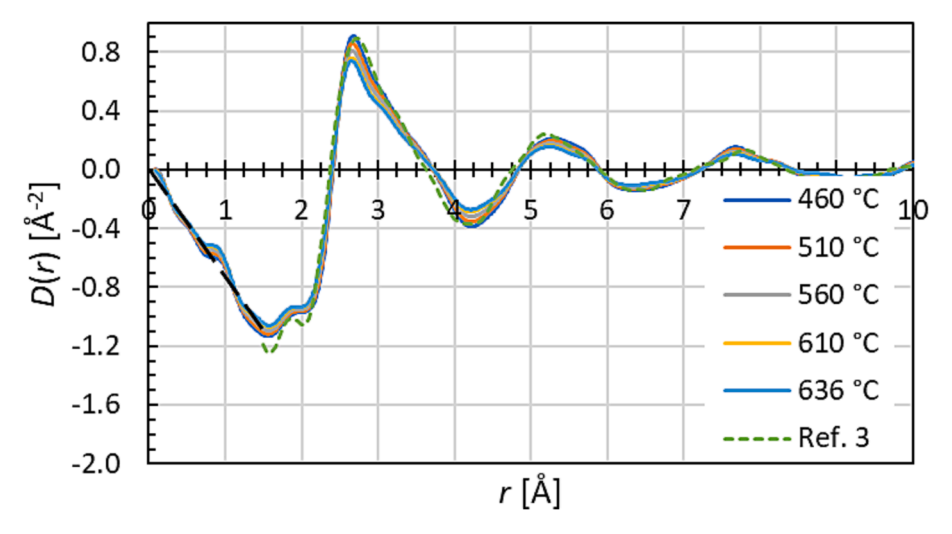
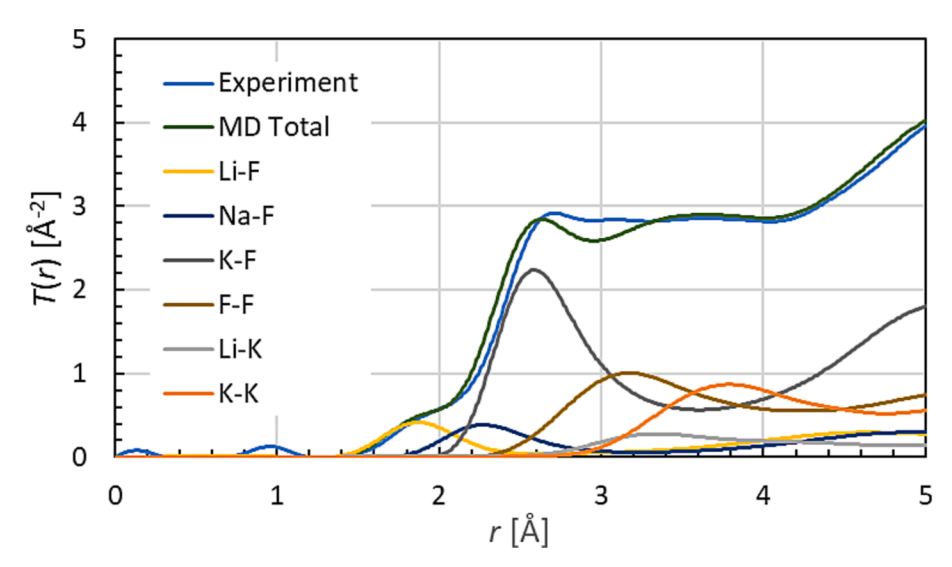


Fig. 2. Evolution of experimental differential correlation function D(r) with temperature. The dashed line shows the results of Igarashi et al., obtained at 520 °C.



**Fig. 3.** Experimental total correlation function T(r) at 510 °C and comparison with T(r) calculated from the MD simulations using the same structure factor weightings and transform cutoff as for the experiment. Also shown from MD results are contributions of prominent species pair correlations to T(r).

instead turn to simulation for further guidance.

#### 4. MD simulations

For simulations, we established a 432 atom FLiNaK supercell with eutectic composition (100 Li atoms, 25Na atoms, 91 K atoms, 216 F atoms) and conducted molecular dynamics simulations using LAMMPS [15]. A Buckingham potential model was used with a radial cutoff of 8 Å [16]. A periodic boundary condition was used to eliminate the boundary effect. An Ewald summation of all electrostatic interactions was performed. The initial ionic configure was built in the KF crystal structure by replacing K atoms with Li and Na to represent the solid state of FLiNaK and assigned velocities randomly according to the Gaussian distribution at 10 K. In MD simulations, the system temperature was gradually raised to the specific temperature during 50,000 steps by using an NPT ensemble, thus keeping the number of atoms constant and fixing the pressure at 0 GPa. After reaching the specific temperature, the system was allowed to continue to equilibrate at temperature for 100,000 steps. The average value of thermodynamic data of the last 20% of steps was used as outputs. The timestep was 0.001 picosecond (ps). Formal charges were used for Li (+1), Na (+1), K (+1), F (-1). During the final equilibration process, the partial pair distribution functions

also were calculated and recorded.

Fig. 4 shows the MD species-specific pair distribution functions  $g_{\alpha\beta}(r)$ at T = 510  $^{\circ}$ C. These are in good agreement with the *ab-initio* MD results of Frandsen *et al.* (cf. Fig. 4b in Frandsen *et al.* [5]). The MD  $g_{\alpha\beta}(r)$  results can be compared with the experimental results through calculation of the predicted x-ray differential and total correlation functions. In order to compare as closely as possible with experiment, Eq. (2) was used to calculate F(q) from the  $g_{\alpha\beta}(r)$ , with a Lorch function which truncated the results at  $q_{max} = 16.0 \text{ Å}^{-1}$  to give a predicted x-ray scattering function F (q). These were then Fourier sine transformed back to real space as per Eqs. (4) and (5) to yield predicted x-ray differential correlation functions D(r) as shown in Fig. 5, as well as the total correlation functions T(r). A comparison of the experimental and MD T(r) results at 510 °C is shown in Fig. 3. In addition, the figure shows the contribution of individual pair correlations to the MD T(r) function. Examination of Fig. 3 shows that the MD K-F and perhaps Na-F distances appear to be slighly shorter than measured and there is slighly more structure near 2.5 and 3.5 Å in the simulation than in the experiment. However, overall agreement between experiment and MD results is very good. The challenge of reliably fitting the experimental results a priori is immediately apparent in Fig. 3 as the there are multiple overlapping contributions to T(r) at most distances and peaks of individual contributions are not Gaussian in profile, further

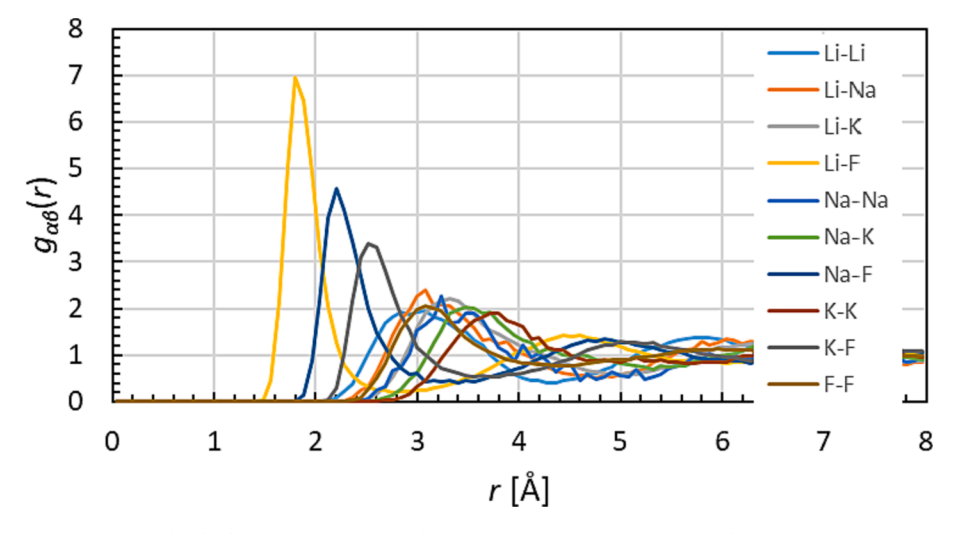


Fig. 4. Individual species-specific pair distribution functions from MD simulations at 510  $^{\circ}\text{C}.$ 

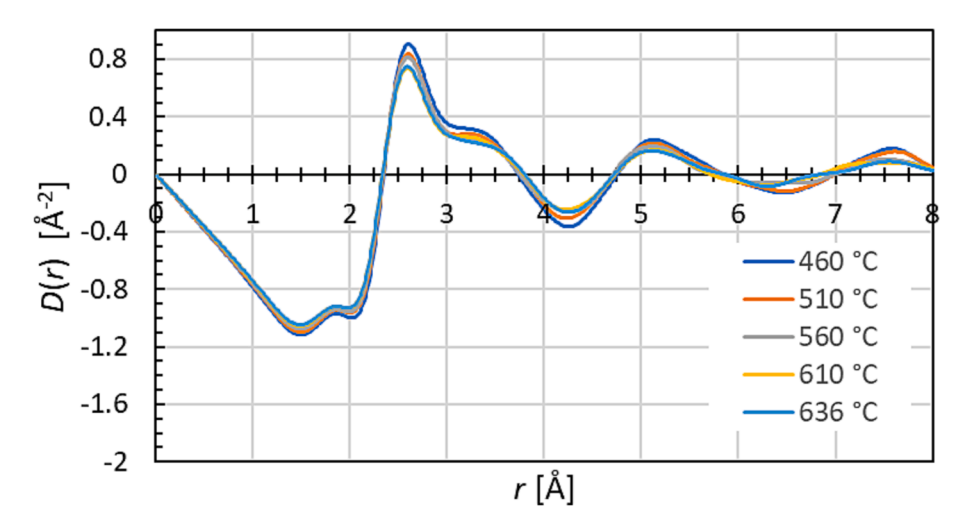


Fig. 5. Predicted x-ray differential correlation functions D(r) calculated from the MD species-specific pair distribution functions.

complicating any fitting process.

# 5. Atomic structure of the liquid

To gain insight into the structure of the liquid, we examine the MD simulations results more closely. Nearest-neighbor cation-anion coordination distances, numbers and root mean square displacements are given in Table 1. The distances are the peaks in the MD cation-anion pair distribution functions  $g_{\alpha\beta}(r)$ ; their uncertainties are approximately  $\pm 0.03 \text{\AA}$ , based on difficulty of identifying the peak position. The coordination numbers and root mean square displacements include contributions up to the first minimum in the  $g_{\alpha\beta}(r)$  functions. The increased

coordination shell width for Na-F and K-F compared to Li-F is easily seen in Fig. 4. Overall, good agreement is seen with previous experiment of Igarashi et al. [3] and recent simulations [5,6]. We note that the *ab-initio* MD (AIMD) simulations of Frandsen *et al.* and Lee *et al.* used 100 atoms while the present simulations use less-accurate classical potentials but with a much larger number of atoms (432 atoms). Lee *et al.* had also found good agreement between smaller AIMD simulations and larger simulations using optimized potentials. The level of consistency between three simulations shows the maturity of MD simulations of the salt despite different methodologies and system sizes. Finally, for later comparison purposes, we also note that the peak in the F-F distribution function is at  $r_{F-F}=3.12\pm0.03\text{\AA}$ .

Table 1
NN cation-anion coordination distances and numbers.

|      | P<br>r [Å] | P<br>N | P<br>σ [Å] | I<br>r [Å] | I<br>N | I<br>σ [Å] | F<br>r [Å] | F<br>N | L<br>N    |
|------|------------|--------|------------|------------|--------|------------|------------|--------|-----------|
| Li-F | 1.83       | 4.0    | 0.23       | 1.83       | 3.3    | 0.177      | 1.84       | 4      | 3.87-4.12 |
| Na-F | 2.21       | 5.4    | 0.32       | 2.18       | 3.8    | 0.261      | 2.2        | 5.42   | 4.57-5.25 |
| K-F  | 2.54       | 6.4    | 0.37       | 2,59       | 4.0    | 0.282      | 2.6        | 7.12   | 7.38-7.78 |

P: Present Work: root mean square displacements  $\sigma$  are calculated using distances up to the first minimum in the  $g_{\alpha\beta}(r)$  functions.

I: Igarashi et al. [3] (x-ray); root mean square displacements are calculated from a Gaussian fit to coordination shells.

F: Frandsen et al. [5] (AIMD).

L: Lee et al. [6] (AIMD and Machine-Learning Optimized MD).

Fig. 6 shows that there is a significant variation in coordination numbers (CNs) within each species, especially for Na-F and K-F pairs. Overall, it's seen that Li is predominantly 4-fold coordinated by F while the median CNs of 5 for Na-F and 7 for K-F, which is consistent with the average CNs. The average coordination numbers observed here and in other simulations follow the same trend with increasing cation size as obtained from fits of x-ray data by Igarashi  $\it et al.$  However, there they reported much less variation with cation, going from CN(Li-F) = 3.3 to CN(Na-F) = 3.8 to CN(K-F) = 4.0. We note that they effectively assumed that each type of NN pair contributes as a Gaussian shell to the total PDF, while we observe here that the pair distributions are actually quite asymmetric. If only the central part of the distribution is included in the calculation, resulting CN's are naturally smaller. In agreement with this supposition, the NN shell widths given in Igarashi  $\it et al.$  [3] are systematically smaller than those reported here (Table 1).

Angular Distribution Functions (ADFs) showing the distribution of bond angles as a function of the polar angle  $\theta$  provide further information about local cation-anion coordination environment. It is also useful to consider the probability of finding an angular correlation per unit solid angle, rather than per unit polar angle  $\theta$ . The angular correlation per unit solid angle is presumably independent of relative azimuthal angle, so the angular correlation per unit solid angle  $P(\theta) = ADF(\theta)/(2\pi sin\theta)$ . The anion-cation–anion nearest-neighbor  $ADF(\theta)$  and  $P(\theta)$  at 510 °C are shown in Fig. 7. These appear to agree well with the MD results of Lee et~al.~[6].

The F-Li-F distributions have a distinct peak at approximately  $105^{\circ}$ –near the  $109.5^{\circ}$  angle of a perfectly tetrahedral coordination around the central Li cation. Moreover, the edge distance in a tetrahedron is  $\sqrt{(8/3)}$  times the center-to-vertex distance. With the observed  $r_{Li-F}=1.83\text{\AA}$ , this predicts  $r_{\text{F-F}}$  is 2.99 Å, in reasonable agreement with the broad  $g_{FF}(r)$  peak centered at 3.12 Å.

The distributions for F-Na-F and F-K-F are much broader. For the F-Na-F angle, there is a peak at around 81° in both ADF( $\theta$ ) and P( $\theta$ ). An octahedral coordination of 6 flourines around a cation, such as is found in the rocksalt crystal structure of LiF, NaF and KF, would give a F-cation-F angle of 90°, which is not too much higher than the observed peak for F-Na-F. Moreover, in P( $\theta$ ) a second broad peak is seen at 180°, again consistent with an octahedral coordination geometry. The edge distance in an octahedron is  $\sqrt{2}$  times the center-to-vertex distance. With the observed  $r_{Na-F}=2.21\text{\AA}$ , this predicts that  $r_{F-F}$  is 3.12 Å, again in agreement with the broad  $g_{FF}(r)$  F-F peak centered at that same value.

For F-K-F bond angles, there is a maximum near  $70^{\circ}$ . The angle for a cube of anions around the central cation (as in the CsCl crystal structure) is  $70.5^{\circ}$ , which is thus the same as observed. However, for F-K-F there is no  $180^{\circ}$  peak observed in  $P(\theta)$ ; nor is there a peak near  $109.5^{\circ}$ , which

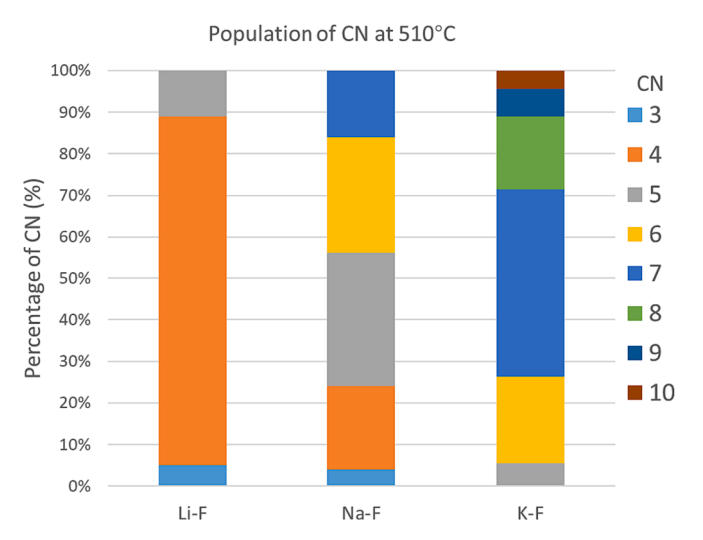


Fig. 6. Histogram of cation-anion coordination numbers at 510 °C.

would be expected for a cube of anions. Instead, there is a rather broad distribution of angles. This indicates the presence of considerable disorder in relative F ion configurations around a K ion. For a cube, the length of an edge is  $2/\sqrt{3}$  times the center-corner distance. With the observed  $r_{K-F}=2.54\text{\AA}$ , this predicts  $r_{F-F}$  is 2.93 Å, yet again in reasonable agreement with the broad  $g_{FF}(r)$  peak centered at 3.12 Å. However, given the lack of peaks at  $109.5^{\circ}$  and  $180^{\circ}$  in ADF( $\theta$ ) and P( $\theta$ ), any "cuboidal" configuration of anions around K<sup>+</sup> must be very disordered.

Fig. 8 shows the distribution of F-F-F bond angles. There is a strong peak just below  $60^{\circ}$ , suggesting local hexagonal arrangements of atoms. However, the  $P(\theta)$  function shows that beyond this peak, the probability of a given configuration is independent of angle, suggesting considerable disorder.

If all neighbors up to the first minimum in the  $g_{FF}(r)$  function are included, the F-F NNN CN is ~11. A similar F-F NNN CN was reported from the simulations of Frandsen et al. [5]. Here we note that this is comparable to the number of neighbors in a dense hard-sphere (HS) liquid. Moreover, the relatively simple shape of the F-F correlation function resulting from the consistent F-F distances around the different cations further suggests comparison with the correlations of a HS liquid using an extended diameter for the F atom to reflect that the anions are physically separated due to their coordination of cations. Fig. 9 shows a comparison with a simple HS liquid calculated using the method of Trokhymchuk et al. [17] and taking atomic diameter  $d_E^{ext} = 2.86\text{Å}$  while using the actual number density of F atoms in the liquid. Also shown is the result of convolving the HS total correlation function T(r) with a gaussian of width  $\sigma=0.22~\mbox{\normalfont\AA}$  to more realistically reflect the nature of atomic interactions. The agreement of the MD F-F correlations with this simple model is striking.

Turning now to the NNN cation-cation correlations, Table 2 shows the calculated number of cation-cation NNNs at 510 °C out to the first minimum of  $g_{\alpha\beta}(r)$ . Total NNN coordination numbers are high and increase with increasing cation size. The right column shows the cation fractions of NNN for each cation central atom; these can be compared with the FLiNaK Li-Na-K cation fractions of 46.5–11.5–42. Relative to the random composition values, there is clear preference for the large K<sup>+</sup> ions to be NNNs around the small Li<sup>+</sup> ions.

Before concluding our discussion of the liquid structure, we compare results from the molten FLiNaK mixture with the structures of the respective individual pure molten salts and their crystalline form. The NN cation-anion distance values in FLiNaK found here and in other recent studies [5] are generally slightly below those reported for the pure molten components in the early work of Zarzycki [18], which reported approximately 2.0 Å for Li-F, for 2.3 Å for Na-F and 2.66 Å for K-F. The experimental values are also slightly below the NN cation—anion distances in the binary crystals at 510 °C (2.05 Å in LiF, 2.33 Å in NaF and 2.68 Å in KF). Among the three cations, the largest difference in coordination distances between FLiNaK melt and crystal is for Li-F pairs, a point to which we will return momentarily.

While all of the binary crystals of NN cation-anion CNs of 6, Zarzycki [18] reported values in the pure molten components which were well under this, though increasing slightly with cation size: (CN(Li-F) = 3.7 to CN(Na-F) = 4.1 to CN(K-F) = 4.9). Although these values and trend are generally consistent with the FLiNaK mixture results of Igarashi  $\it et~al.$  [3], they are systematically a bit lower than the FLiNaK mixture results found here (CN(Li-F) = 4.0 to CN(Na-F) = 5.4 to CN(K-F) = 6.4) and reported in other recent simulations.

The overall picture from the comparison with the binary crystals is that melting to the FLiNaK mixture frees the cation-ion NNs to relax closer together, with the decrease in NN distance being largest for Li-F pairs. Concommitantly, the cation-anion CN is freed from the crystal value of 6, with the largest change again being the decrease from 6 to 4 for Li-F pairs.

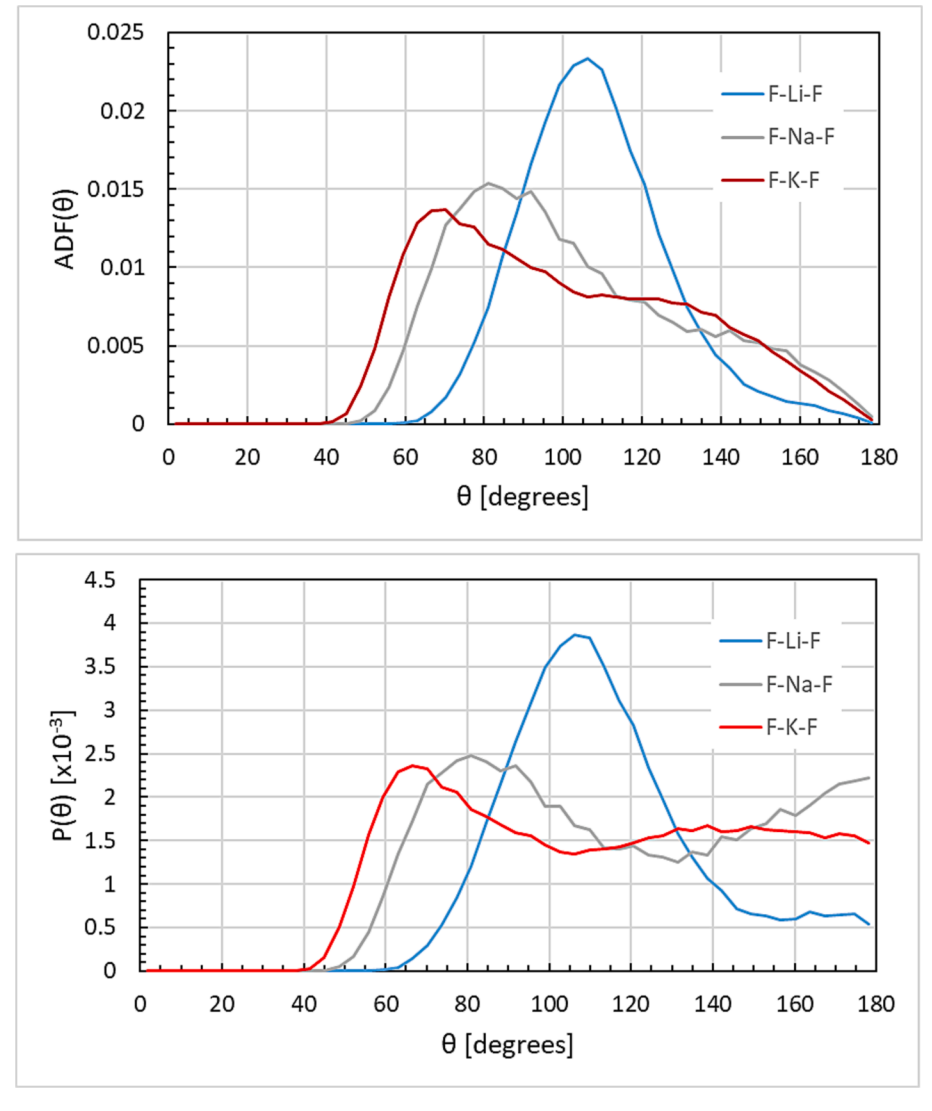


Fig. 7. Nearest-neighbor bond angular distributions at 510 °C calculated from MD simulations.

#### 6. Temperature dependence of structure

Both the experimental and MD real-space correlation functions of Figs. 2 and 5 respectively show that there is a steady general decrease in correlations with increasing temperature, as expected. However, the experimental and MD results allow us to understand this process in detail. The top of Fig. 10 shows the difference between experimental total correlation functions T(r) at elevated temperatures as compared to T(r)at 460 °C, i.e.  $\Delta$  T(r). The dotted lines represent the change in T(r)due to decrease in average density with increasing temperature. It's immediately apparent that the NN cation-anion structure which occurs in the range of 1.83-2.64 Å is much less affected by increasing temperature than would be suggested by the change in overall density of the melt. However, there is a small positive bump near 2.0 Å and a small negative dip near 2.3 Å. There is a much larger change in local structure in the range from about 2.5 Å to 3.6 Å. These distances correspond to K-F, F-F and cation-cation NNNs. Then, in the range near 4.25 Å there is little change in experimental T(r) with respect to temperature. Above this distance, T(r) again changes significantly with temperature. The bottom of Fig. 10 shows the differences in T(r) calculated for the MD simulations, again using the same treatment as for the experimental T (r). The T(r) differences from the MD simulations show more detail, but the overall shape is the same as observed for the experimental curves – a small bump near 1.9 Å and dip near 2.3 Å, relatively large changes with

temperature from about 2.5 Å to 3.6 Å, and then a region of little change in the total T(r) near 4.25 Å. We therefore turn to the behavior of the individual atomic pair distributions from MD with some confidence.

It's easiest to understand the changes in the  $\mathit{T(r)}$  distribution functions by looking at the individual pair differences  $\Delta g_{\alpha\beta} = \{g_{\alpha\beta}(460~^{\circ}\text{C}) - g_{\alpha\beta}(636~^{\circ}\text{C})\}$ , which are exhibited in Fig. 11. In general, the correlation functions show curves characteristic of an increase in asymmetric peak width with increasing temperature. This is most easily seen around the first peak in the cation-anion functions (top plot of Fig. 11). With increasing r, there is, first, a small negative bump just below the NN peak because in this range there is increased correlation weight with increasing temperature due to the increase in peak width. Then, near the center of the NN peak itself,  $\Delta g_{\alpha\beta}$  is strongly positive because there is loss of weight in the central peak with increasing temperature. Finally, at larger r, there is a broad negative region, again because of the increase in width of the asymmetric peak with increasing temperature.

Also included in the middle plot of Fig. 11 is a further comparison of the MD F-F correlations with the model based on a HS liquid. The dashed line is the difference for the HS liquid model described above between using 1) the F-F density at 460  $^{\circ}\text{C}$  with convolution gaussian of width 0.22 Å and 2) the F-F density at 636  $^{\circ}\text{C}$  with convolution gaussian of width 0.26 Å. The fundamental structural evolution with increasing temperature is reproduced and appears to be determined again by broadening of the asymmetric first coordination peak.

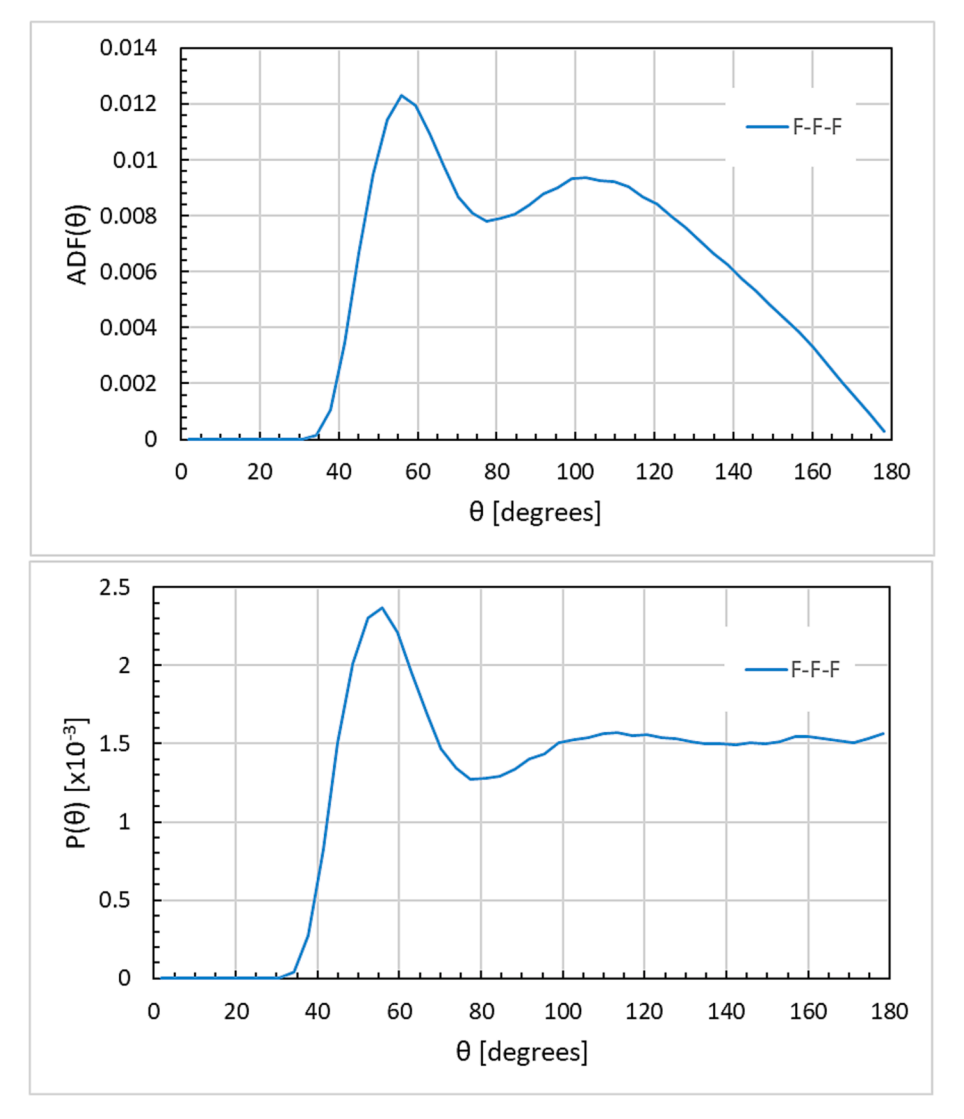


Fig. 8. F-F-F bond angular distributions at 510  $^{\circ}\text{C}$  calculated from MD simulations.

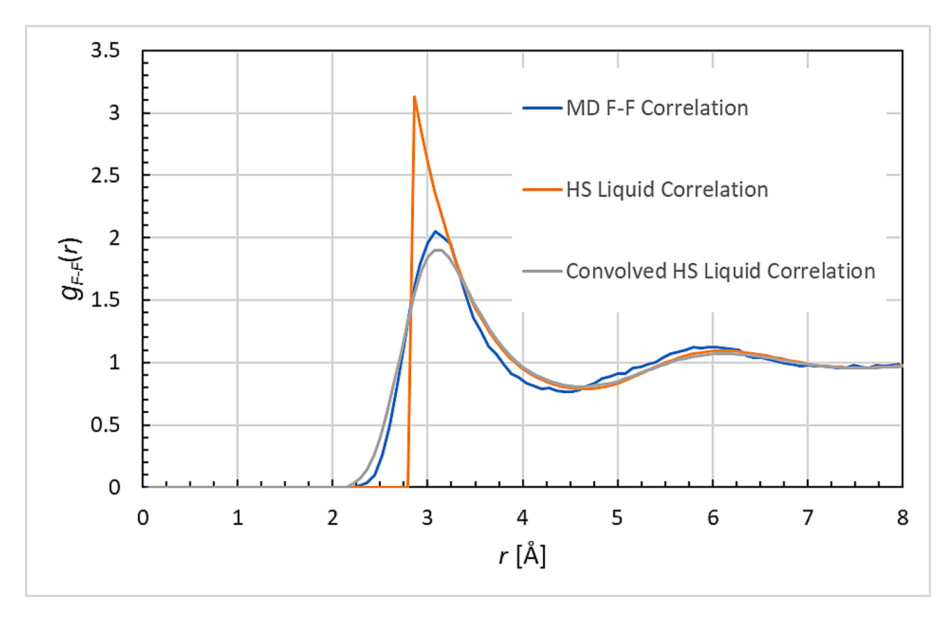


Fig. 9. Comparison of MD F-F NNN correlations with Hard Sphere (HS) liquid models.

Table 2
NNN cation-cation coordination numbers and atomic species fractions.

|                 | Coordinating<br>Atom | Li  | Na  | K   | Total<br>NNN CN<br>Number | Li-Na-K<br>Fractions<br>46.5–11.5–42.0 |
|-----------------|----------------------|-----|-----|-----|---------------------------|--|
| Central<br>Atom |                      |     |     |     |                           |  |
| Li              |                      | 4.5 | 1.6 | 6.5 | 12.6                      | 0.35-0.13-0.52                         |
| Na              |                      | 6.5 | 1.4 | 7.7 | 15.6                      | 0.41-0.09-0.50                         |
| K               |                      | 7.2 | 2.1 | 7.5 | 16.8                      | 0.43-0.12-0.45                         |

We can now understand the temperature changes in the experimental T(r), remembering that the dominant contributions come from K-F, K-K and F-F correlations. The small bump in  $\Delta T(r)$  at 2.0 Å is due to decrease in the center of the Li-F correlations with increasing temperature. The negative dip near 2.3 Å is due primarily to the increasing width of K-F correlations. The large positive region of 2.5–3.6 Å is due largely to the decreasing correlations at the center of the K-F, K-K and F-F distributions. Then, the dip in  $\Delta T(r)$  near 4.25 Å is due to the increasing width of the K-F, K-K and F-F distributions with increasing temperature, adding additional correlation weight in this region which counteracts the decreasing overall density.

#### 7. Discussion and conclusions

As discussed above, there are several key motifs in the FLiNaK

structure. In accord with previous studies [3,5,6], these include:

- Nearest-neighbor cation-anion distances increasing with cation size and slightly shorter than in the crystals of the respective components.
- 2) Increasing average NN cation-anion CN with increasing cation size. CNs increase from ∼4 for Li-F, to ∼5.4 for Na-F, to above 6 for K-F.

However, by examining carefully the MD results, we also find evidence for more detailed structural elements:

- 3) Different typical geometries of anions about the cations going from tetrahedral for Li-F to octahedral for Na to very disordered "quasicuboidal" for K.
- 4) Different geometries and coordination distances around the different cation species causing a relatively fixed F-F NNN distance of approximately 3.1 Å. This allows the F anions to assume an overall structure very similar to that of a HS liquid with an extended radius beyond the normal F ion size due to the cation-anion coordination requirements. Within the temperature range studied, the evolution of F-F correlations with increasing temperature is consistent with changes expected in a HS liquid simply due to decreasing density. The importance of F-F correlations is consistent with the high concentration of F<sup>-</sup> anions in the melt and the relatively high volume fraction that they occupy (approximately 46% of all occupied volume, using typical ionic radius values [19]).

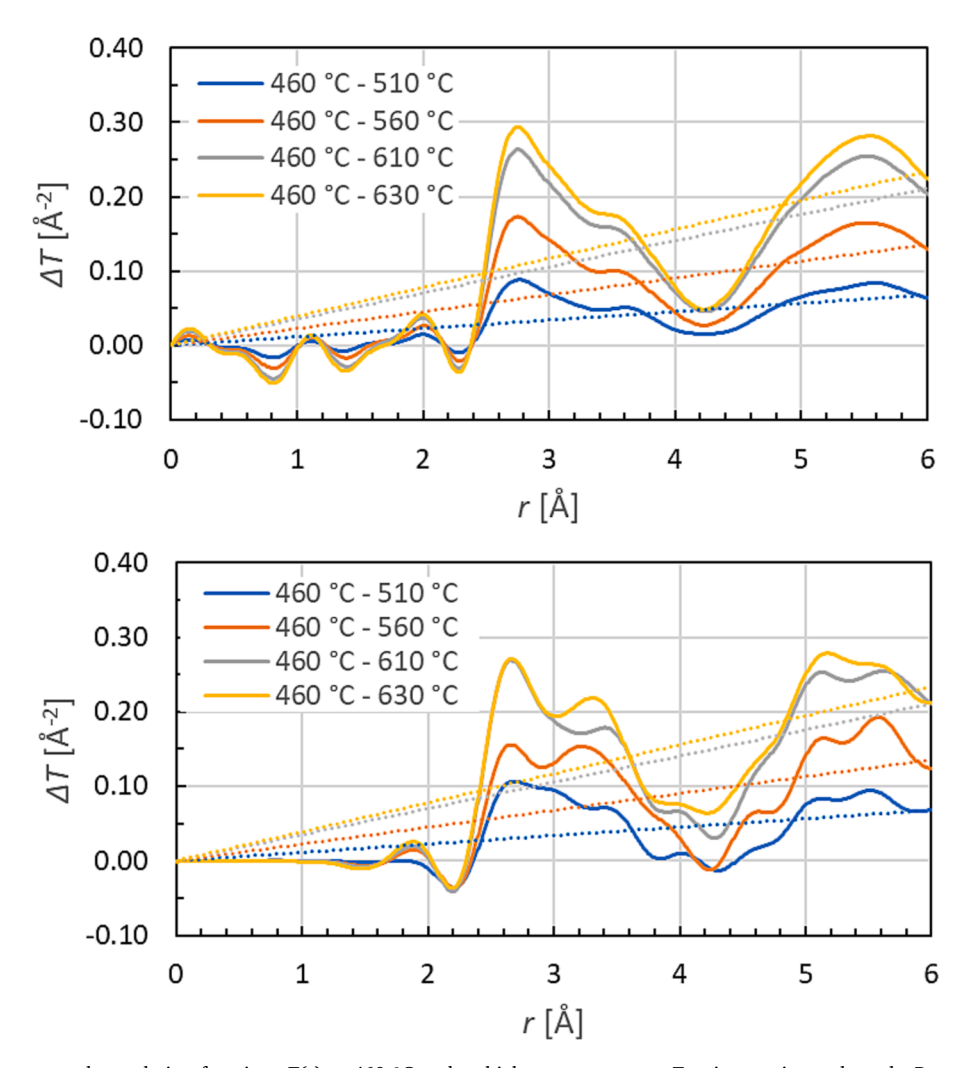


**Fig. 10.** Differences between total correlation functions T(r) at 460 °C and at higher temperatures. Top is experimental result. Bottom is calculated from MD simulations. The dotted lines are the contributions due to changing density with increasing temperature.

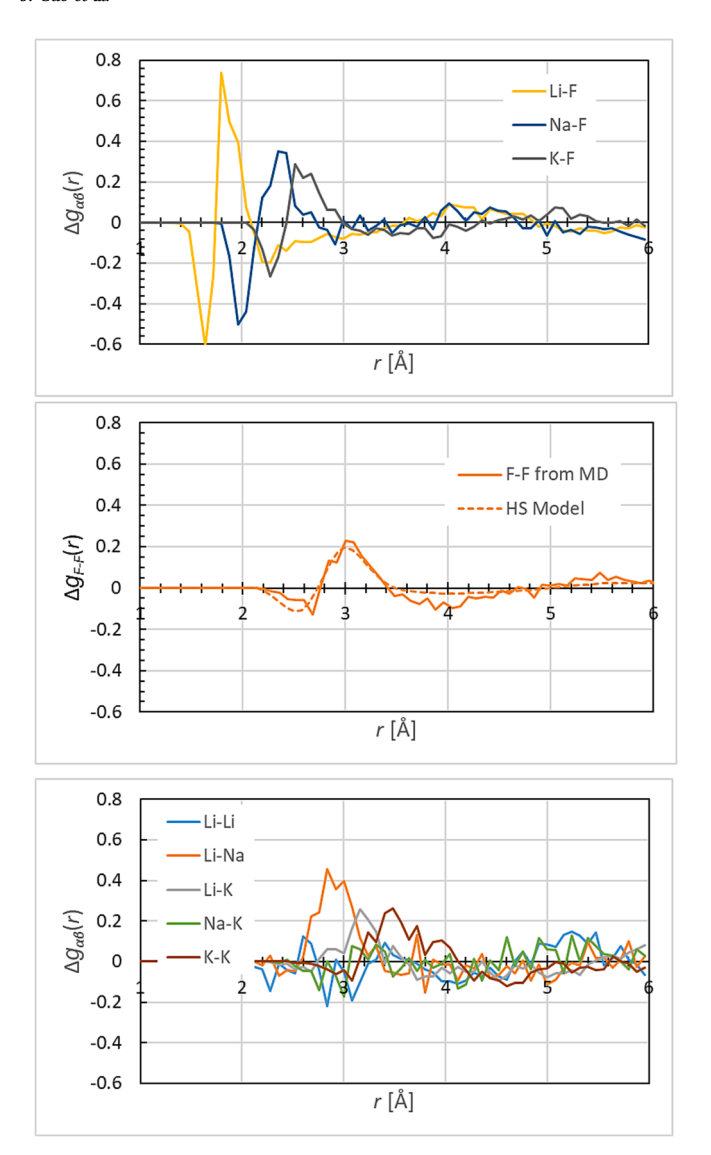


**Fig. 11.** Differences in pair correlation functions between 460  $^{\circ}$ C and 636  $^{\circ}$ C for (top) cation-anion pairs, (middle) F-F anion pairs, and (bottom) cation-cation pairs. The dashed line compares the F-F change to that predicted based on a HS model as discussed in the text. The Na-Na correlation is very noisy and is not shown in the bottom plot to preserve clarity.

5) Some preference for large K<sup>+</sup> ions to be NNNs around the small Li<sup>+</sup> ions relative to the average composition.

Moreover, careful consideration of the evolution of the experimental atomic distribution functions with increasing temperature shows that the changes in correlation at each distance can be understood within the context of broadening asymmetric neighbor distributions. No fundamental change in liquid structure is observed in this temperature range. It has been reported from previous MD calculations that the NN cationanion distance in pure molten alkali halide salts *decreases* slightly with increasing temperature [20,21,22]. In the present study, clear changes to the NN distances are not observed, perhaps due to the limited maximum temperature of 636  $^{\circ}$ C. It would be quite interesting to probe the structural evolution with higher temperatures.

An interesting comparison is possible with oxide liquids and glasses, for which cation field strength  $FS = Z_{cat}/(r_{cat-an} - r_{an})^2$  has been shown to play an important role in relative structure [23]. Here  $Z_{cat}$  is the formal charge on the cation,  $r_{cat-an}$  is the cation-anion NN distance and  $r_{an}$  is the anion ionic radius. Within the FLiNaK salt, we expect  $FS_{Li} > FS_{Na} > FS_K$ 

because of the increasing cation size. In the oxide melts, larger cations with lower FS are observed to have larger cation-anion NN CNs and more disordered, asymmetric coordination shells [23]. This is consistent with what is observed within the single FLiNak salt for the different anions. On the other hand, in the oxide melts it's observed that the drop in CN in going from the crystal to the liquid is larger for lower FS, while within the FLiNaK salt there is considerable decrease in Li-F CN relative to the pure crystal while the K-F CN is larger than in the crystal. So here the correlation of CN with cation field strength observed in oxide melts does not hold. Rather steric effects associated with the cation size seem likely to be a dominant factor.

Considering the anion structure of the liquid, we note that, for a given density, the structure of a true HS liquid is driven only by entropy. Given the reasonable agreement of the simple extended and broadened hard sphere model for the F-F correlations with the MD results, this suggests that the configuration of F ions made possible by the relatively fixed F-F NNN distance independent of neighboring cation in FLiNaK yields a particularly favorable entropy.

# CRediT authorship contribution statement

**Jicheng Guo:** Investigation, Formal analysis, Writing – review & editing. Yifan Zhang: Investigation, Formal analysis, Writing - review & editing. Karl Ludwig: Conceptualization, Methodology, Formal analysis, Writing - original draft, Supervision, Funding acquisition. Haoxuan Yan: Investigation, Writing - review & editing. Alexander Levy: Investigation, Writing - review & editing. Anubhav Wadehra: Investigation, Writing – review & editing. Michael Gao: Methodology, Writing - review & editing. Chris Benmore: Investigation, Formal analysis, Writing - review & editing. Melissa Rose: Investigation, Writing - review & editing. Nicholas Condon: Conceptualization, Writing - review & editing, Supervision, Project administration, Funding acquisition. Adam Powell: Conceptualization, Writing - review & editing, Supervision, Project administration, Funding acquisition. Yu **Zhong:** Conceptualization, Methodology, Writing – review & editing, Supervision, Project administration, Funding acquisition. Uday Pal: Conceptualization, Writing - review & editing, Supervision, Project administration, Funding acquisition.

# **Declaration of Competing Interest**

The authors declare that they have no known competing financial interests or personal relationships that could have appeared to influence the work reported in this paper.

#### Data availability

Data will be made available on request.

# Acknowledgements

This research at Boston University and the Worcester Polytechnic Institute was supported by the US Department of Energy (DOE) NEUP program [Grant Number 20-19373] and the US National Science Foundation (NSF) [Award No. CMMI-1937818]. This research used resources of the Advanced Photon Source, a U.S. Department of Energy (DOE) Office of Science user facility operated for the DOE Office of Science by Argonne National Laboratory under Contract No. DE-AC02-06CH11357.

#### References

[1] J. Serp, M. Allibert, O. Benes, S. Delpech, O. Feynberg, V. Ghetta, D. Heuer, D. Holcomb, V. Ignatiev, J.L. Kloosterman, L. Luzzi, E. Merle-Lucotte, J. Uhlir, R. Yoshioka, D. Zhimin, The molten salt reactor (MSR) in generation IV: Overview and perspectives, Prog. Nucl. Energy 77 (2014) 308–319, https://doi.org/10.1016/ i.pnucene.2014.02.014.

- [2] M. Liu, N.H.S. Tay, S. Bell, M. Belushko, R. Jacob, G. Will, W. Saman, F. Bruno, Review on concentration solar power plants and new developments in high temperature thermal energy storage technologies, Renew. Sustain. Energy Rev. 53 (2016) 1411–1432, https://doi.org/10.1016/j.rser.2015.09.026.
- [3] K. Igarashi, Y. Okamoto, J. Mochinaga, H. Ohno, X-ray Diffraction Study of Molten Eutectic LiF-NaF-KF Mixture, J. Chem. Soc., Faraday Trans. 84 (1) (1988) 4407, https://doi.org/10.1039/F19888404407.
- [4] D. Sprouster, G. Zheng, S.-C. Lee, D. Olds, C. Agca, J. McFarlane, Y. Z, B. Khaykovich, Molecular Structure and Phase Equilibria of Molten Fluoride Salt with and without Dissolved Cesium: FLiNaK-Cs (5 mol%), ACS Appl. Energy Matter. 5 (2022) 8067.
- [5] B.A. Frandsen, S.D. Nickerson, A.D. Clark, A. Solano, R. Baral, J. Williams, J. Neuefeind, M. Memmott, The Structure of Molten FLiNaK, J. Nucl. Mater. 537 (2020), 152219, https://doi.org/10.1016/j.jnucmat.2020.152219.
- [6] S.-C. Lee, Y. Zhai, Z. Li, N.P. Walter, M. Rose, B.J. Heuser, Y. Z., Comparative Studies of the Structural and Transport Properties of Molten Salt FLiNaK Using the Machine-Learned Neural Network and Reparametrized Classical Forcefields, J. Phys. Chem. B 125 (2021) 10562, https://doi.org/10.1021/acs.jpcb.1c05608.
- [7] D.O. Zakiryaov, The FLiNaK-CeF<sub>3</sub> molten mixture: A Comprehensive Structure Examination by Means of Ab Initio Molecular Dynamics, J. Mol. Liquids 360 (2022), 119400, https://doi.org/10.1016/j.molliq.2022.119400.
- [8] X. Li, T. Xu, M. Liu, Y. Zuo, Diffusion Behaviors of HF in Molten LiF-BeF<sub>2</sub> and LiF-NaF-KF Eutectics Studied by FPMD Simulatnios and Electrochemical Techniques, J. Nucl. Mater. 572 (2022), 154031.
- [9] J. Guo, A. Merwin, C.J. Benmore, Z.-G. Mei, N.C. Hoyt, M.A. Williamson, Fluid Structure of Molten LiCl-Li Solutions, J. Phys. Chem. B 123 (2019) 10036, https://doi.org/10.1021/acs.jpcb.9b07479.
- [10] A.P. Hammersley, S.O. Svensson, M. Hanfland, A.N. Fitch, D. Häusermann, Two-Dimensional Detector Software: From Real Detector to Idealised Image or Two-Theta Scan, High Pressure Res. 14 (1996) 235, https://doi.org/10.1080/08957959608201408
- [11] X. Qiu, J.W. Thompson, S.J.L. Billinge, PDFgetX2: A GUI driven program to obtain the pair distribution function from X-ray powder diffraction data, J. Appl. Cryst. 37 (2004) 678, https://doi.org/10.1107/S0021889804011744.
- [12] E. Lorch, Neutron Diffraction by Germania, Silica and Radiation-Damaged Silica Glass, J. Phys. C Solid State Phys. 2 (1969) 229.

- [13] D.A. Keen, A Comparison of Various Commonly Used Correlation Functions for Describing Total Scattering, J. Appl. Cryst. 34 (2001) 172, https://doi.org/ 10.1107/\$0021889800019993.
- [14] M. Chernková, V. Daněk, R. Vasiljev, A. Silny, V. Kremenetsky, E. Polyakov, Density and Viscosity of the (LiF-NaF-KF)<sub>eut</sub>-KBF<sub>4</sub>-B<sub>2</sub>O<sub>3</sub> Melts, J. Mol. Liquids 102 (2003) 213, https://doi.org/10.1016/S0167-7322(02)00063-6.
- [15] A.P. Thompson, H.M. Aktulga, R. Berger, D.S. Bolintineanu, W.M. Brown, P. S. Crozier, P.J. in't eld, A. Kohlmeyer, S.G. Moore, T.D. Nguyen, R. Shan, M. J. Stevens, J. Tranchida, C. Trott, S.J. Plimpton, LAMMPS a flexible simulation tool for particle-based materials modeling at the atomic, meso, and continuum scales, Comp. Phys. Commun. 271 (2022) 10817, https://doi.org/10.1016/j.cre.2021.10817.
- [16] M. Salanne, C. Simon, P. Turq, P.A. Madden, Heat-transport properties of molten fluorides: Determination from first-principles, J. Fluor. Chem. 130 (1) (2009) 38–44, https://doi.org/10.1016/j.jfluchem.2008.07.013.
- [17] A. Trokhymchuk, I. Nezbeda, J. Jirsák and D. Henderson, Hard-Sphere Radial Distribution Function Again, J. Chem. Phys. 123 (2005) 024501; Erratum: J. Chem. Phys. 124 (2006) 149902. doi: 10.1063/1.1979488.
- [18] J. Zarzycki, Étude des Sels fondus Par Diffraction des Rayons X aus Températures Élevées. I. Structure a L'état Liquide des Fluorures LiF, NaF et KF, J. Phys. Phys. Appl. 18 (S7) (1957) 65, https://doi.org/10.1051/jphysap:0195700180706500.
- [19] R.D. Shannon, Revised effective ionic radii and systematic studies of interatomic distances in halides and chalcogenides, Acta Cryst. A32 (1976) 751, https://doi. org/10.1107/\$0567739476001551.
- [20] M.-M. Walz, D. van der Spoel, Molten Alkali Halides Temperature Dependence of Structure, Dynamics and Thermodynamics, Phys. Chem. Chem. Phys. 21 (2019) 18516, https://doi.org/10.1039/c9cp03603b.
- [21] S. Tovey, A.N. Krishnamoorthy, G. Sivaraman, J. Guo, C. Benmore, A. Heuer, C. Holm, DFT Accurate Interatomic Potential for Molten NaCl from Machine Learning, J. Phys. Chem. C 124 (2020) 25760, https://doi.org/10.1021/acs. jpcc.0e08870.
- [22] G. Sivaraman, J. Guo, L. Ward, N. Hoyt, M. Williamson, I. Foster, C. Benmore, N. Jackson, Automated Development of Molten Salt Machine Learning Potentials: Application to LiCl, J. Phys. Chem. Lett. 12 (2021) 4278, https://doi.org/10.1021/acs.jpclett.1c00901.
- [23] L.B. Skinner, C.J. Benmore, J.K.R. Weber, J. Du, J. Neuefeind, S.K. Tumber, J. B. Parise, Low Cation Coordination in Oxide Melts, Phys. Rev. Lett. 112 (2014), 147801, https://doi.org/10.1103/PhysRevLett.112.157801.